Structure of the New Hebrides Arc-Trench System

Bernard Michel

A. K. IBRAHIM,[1] B. PONTOISE,[2] G. LATHAM,[1] M. LARUE,[2]
T. CHEN,[1] B. ISACKS,[3] J. RECY,[2] AND R. LOUAT[2]

Jacques

Results from refraction experiments have been combined with local earthquake data to produce a preliminary model for the structure of the New Hebrides arc-trench system. Maximum crustal thickness of about 28 km occurs beneath the island ridge. The crust is unusually thick (about 10 km) in the zone seaward (westward) of the trench, where the velocity of the deepest layer is 7.0 km/s. The crustal thickness of the Fiji plateau, east of the New Hebrides ridge, varies between 5 and 7 km. The velocities of the ma terials that form the inner trench wall are similar to those found in the island ridge. A zone of relatively high velocity (4.1 km/s) is encountered at a depth of about 1 km beneath the arc-trench slope. This zone thickens toward the trench and is overlain by material with velocity typical of surficial sediments (≈2 km/s). This may be an accretionary deposit, or it may be of volcanic origin.

INTRODUCTION

The region that includes the New Hebrides and Tonga Island arcs and adjacent oceanic trenches is regarded by many as one of the best natural laboratories available for investigation of plate convergence. While the Tonga region is ideal for the study of a Benioff zone which extends to great depths, the New Hebrides is an example of a shallower Benioff zone which has enough adjacent islands so that the deformation of the overlying lithosphere can be considered in detail. Both active and fossil back arc spreading zones, as well as opposed and oblique convergence zones, can be identified in the region.

A cooperative program has been conducted in this region over the past three years by the Office de la Recherche Scientifique et Technique Outre-Mer (ORSTOM), Cornell University, and the University of Texas, Marine Science Institute.

[1] Marine Science Institute, Geophysics Laboratory. University of Texas, Galveston, Texas 77550.
[2] Office de la Recherche Scientifique et Technique Outre-Mer, Noumea, New Caledonia.
[3] Department of Geological Sciences, Cornell University, Ithaca, New York 14850.

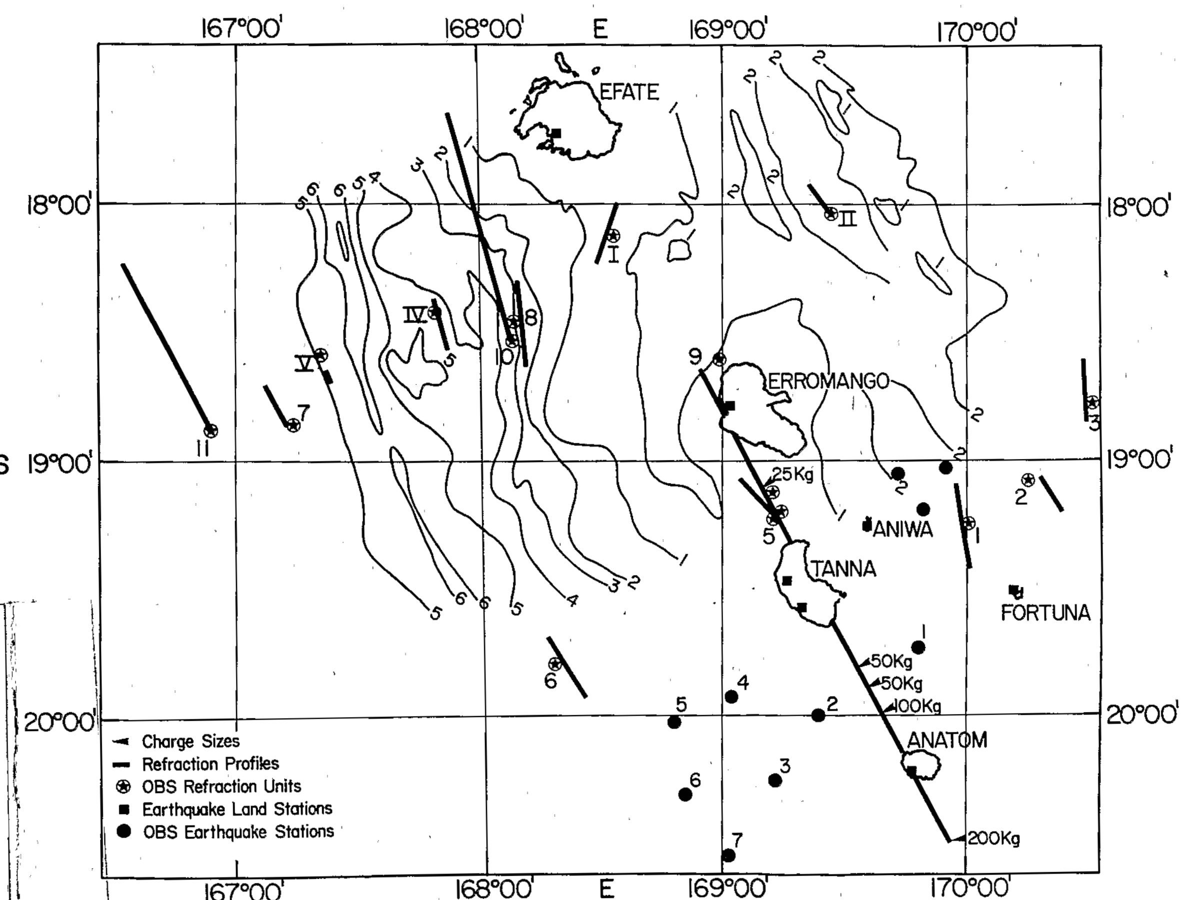

Fig. 1. Map of the central New Hebrides islands showing the locations of OBS stations, land stations, and refraction lines described in this paper. Bathymetric contours (in kilometers) are from the ORSTOM data bank.

Paper number 9B1270.
0148-0227/80/009B-1270-01.00

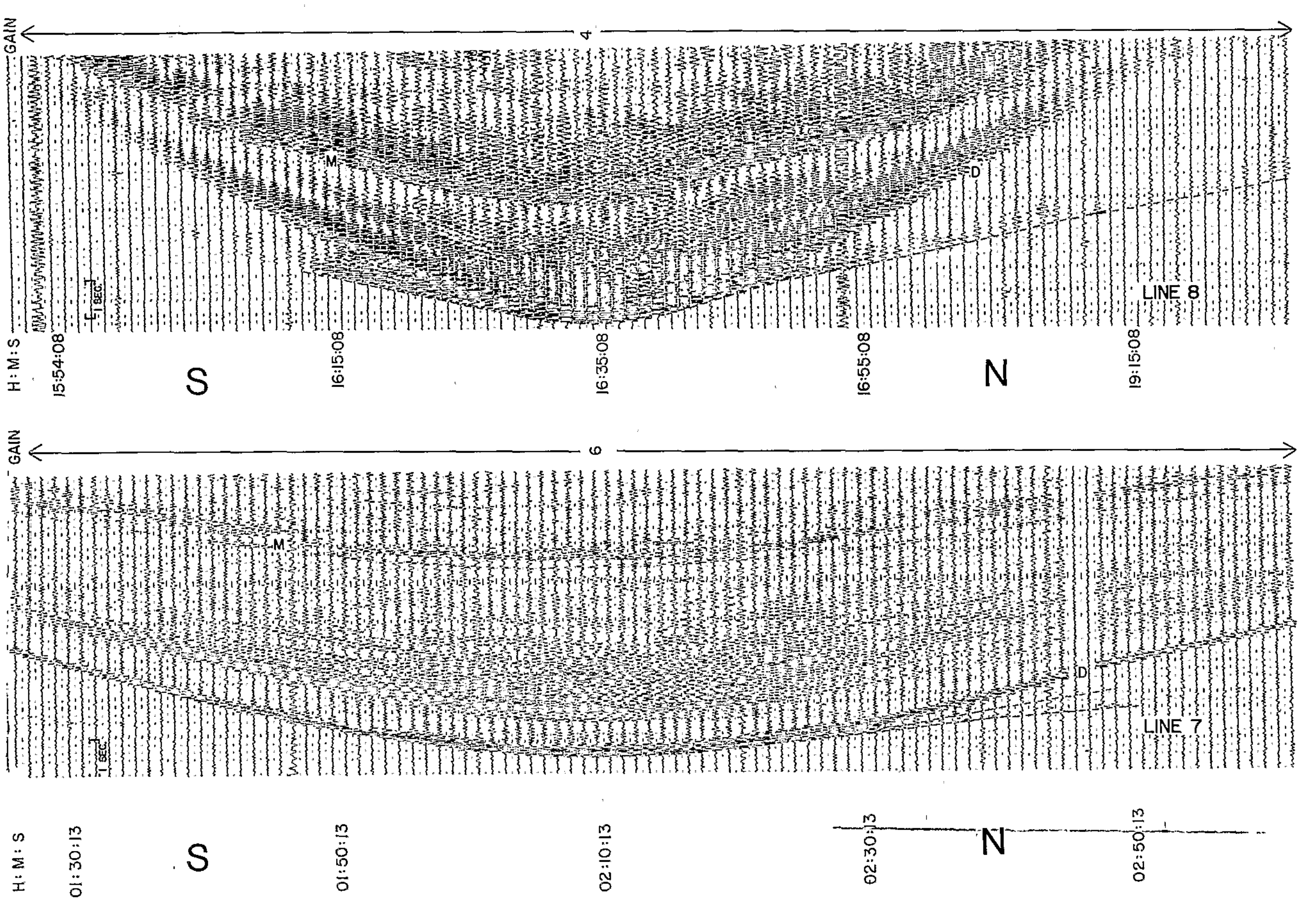

Fig. 2. Examples of record sections used in the analysis of refraction data. The data in this figure and the record sections of Figures 16–20 were plotted assuming that the ship was steaming at a constant speed and the air gun fired once per minute. Assuming the ship was steaming at 8 knots (15 km/h), the separation between each trace would be 0.25 km. H:M:S represents the time of the first data point of each trace. Gain is the gain factor applied to each trace, and it is increased in steps of 6 dB; a constant value indicates the same gain was applied to the whole section. The source for line 7 was a Flexichoc imploding drum. The source for line 8 was a single 5-l air gun fired at a pressure of 138 bars. *D* refers to the direct water wave, *M* denotes multiple reflection in the water column, and dashed lines represent ground arrivals. The 1.0-s arrivals after the water wave in Figure 7 are reflected refracted arrivals.

The program was joined by the National Ocean Survey of NOAA in 1978. As part of this program, refraction seismic surveys and earthquake monitoring experiments have been conducted using both island and ocean bottom seismic (OBS) stations. Data from the 1978 experiments are presently under analysis. Results from the refraction experiments of 1976 and 1977 are presented in this paper.

In the initial field program (summer 1976), a series of four short refraction lines were run in the central New Hebrides at locations indicated by roman numbers in Figure 1. The en-

TABLE 1. OBS Location, Source Type, Water Depth, Maximum Range of Signal Detection, and Shot Interval for Refraction Profiles

Line	OBS Position	Energy Source	Water Depth, km	Maximum Range North, km	Maximum Range South, km	Shot Interval, min
I	18°07.8′S,168°31.0′E	air gun	0.805	14	11	1
II	18°02.0′S,169°26.0′E	air gun	2.615	13		1
IV	18°27.0′S,167°50.0′E	air gun	4.316	14		1
V	18°36.0′S,167°20.8′E	air gun	4.829	13		1
1	19°17.0′S,169°59.0′E	air gun	2.387	20	16	1
2	19°05.5′S,170°17.0′E	air gun	2.122		17	1
3	18°47.0′S,170°30.0′E	air gun	3.009	18	6	1
5	19°00.0′S,169°10.0′E	air gun	0.732	18		1
6	19°47.5′S,168°18.6′E	air gun	5.121	12	18	1
7	18°51.8′S,167°14.0′E	Flexichoc	4.307	12		1
8	18°28.7′S,168°09.8′E	air gun	2.579	17	18	1
9	Figure 1					
10	18°30.8′S,168°08.0′E	dynamite	2.862	100		10
11	18°51.9′S,166°53.4′E	dynamite	4.133	75		10

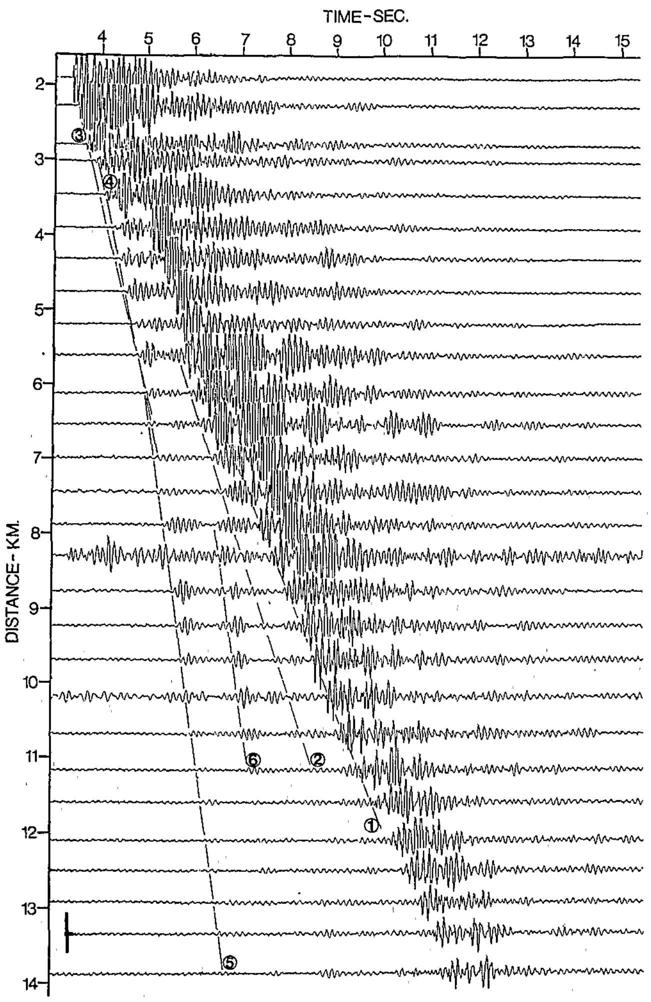

Fig. 3. Record section for line I. Small earthquakes were recorded at distances of 8.3 and 10.2 km. Velocities are given in Figure 4. Note branch 6 is a multiple of branch 5 corresponding to an additional two-way travel time in the water layer.

ergy source for these lines was a single 5-l air gun fired at a 1-min repetition rate at a pressure of 138 bars. This gave detectable arrivals to a maximum range of between 15 and 20 km.

In 1977, seven additional air gun lines, a line using the french Flexichoc source, and three longer lines, using explosion sources, were obtained. These are indicated by numbers 1–11 in Figure 1. A network of eight OBS stations and seven island stations was also installed in 1977 to record local earthquakes. Approximately 500 earthquakes were recorded by this network in 35 days of operation. A short experiment, in which three closely spaced OBS stations were installed in the back arc basin (Coriolis Trough) east of Tanna, showed this zone to be extremely active. Approximately 150 earthquakes were recorded in this zone in a 1-day period.

All of the refraction lines are oriented parallel to the strike of the arc-trench system. In most cases the OBS was deployed, and the ship proceeded to one end of the line as the OBS dropped to the bottom. Shots were fired as the ship moved toward the OBS (usually toward the northwest to maintain a following sea) and continued over and beyond the OBS to the maximum expected range of detection, to produce a split profile. In some shallow water cases, and where explosives were used, shooting began at the OBS drop site and continued on one side of the OBS to produce a single-ended profile. In the air gun and Flexichoc lines the ground arrivals are normally much stronger along the outbound line than they are along the inbound line. This effect is presumably related to the radiation patterns of these sources. Thus in some cases we will present data from both sides of the OBS but will omit data from the inbound leg in cases where signals from this portion of the line are too weak to be useful.

The OBS units used in this study have been described by *Latham et al.* [1978] and *Ibrahim and Latham* [1978]. The refraction units contain a single vertical-component geophone with a resonant frequency of 8 Hz. On command from an internal clock, a 40-s sample of data is stored in memory and then recorded (FM) on magnetic tape along with a time code and reference frequency. The shot clock is initially synchro-

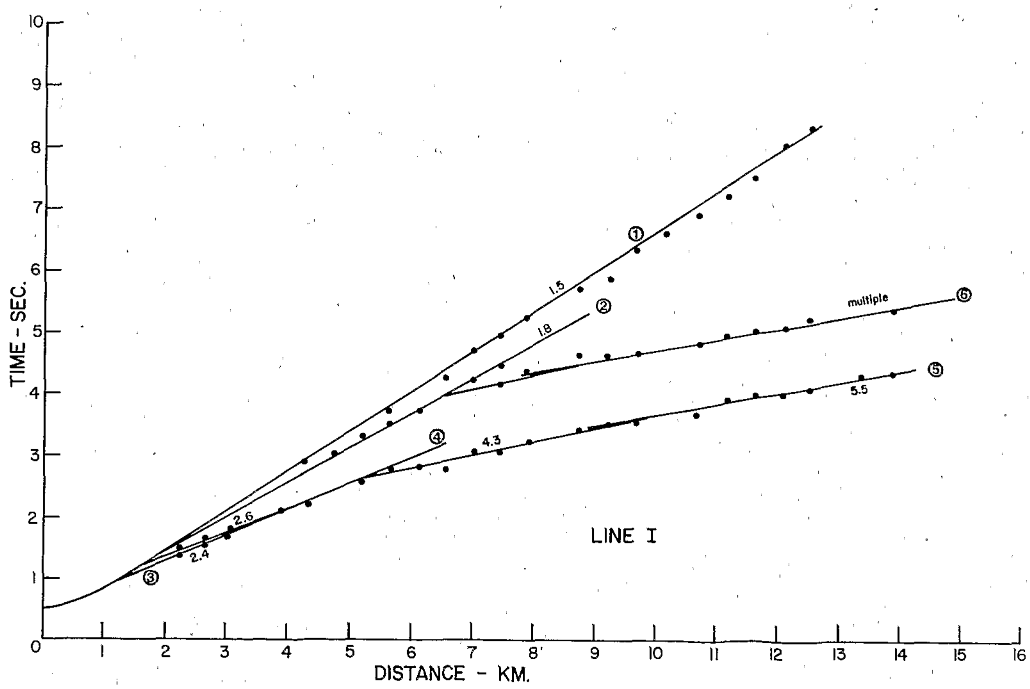

Fig. 4. Travel time curve for line I.

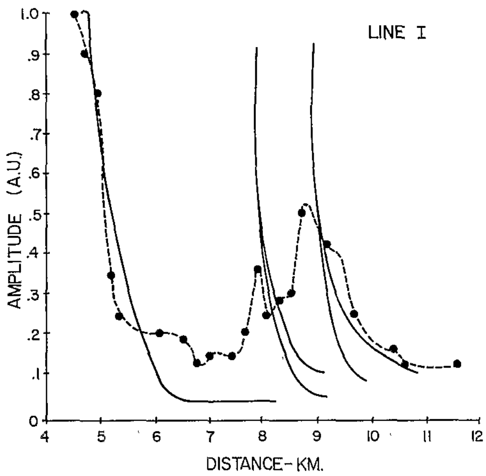

Fig. 5. Calculated (solid line) and observed first arrivals (dashed line) amplitude-distance curves for line I. The model used for calculation is shown in Figure 15.

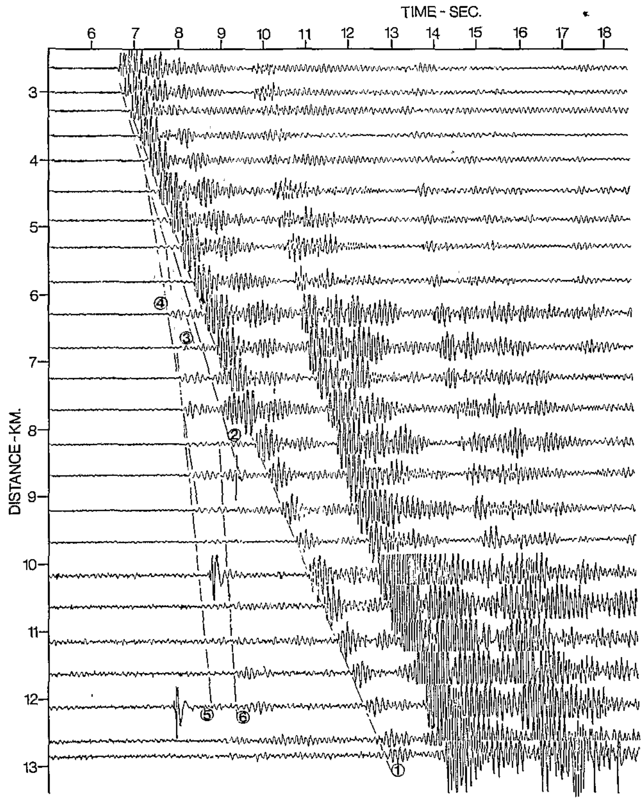

Fig. 6. Record section for line II. Transients caused by bad memory cells within the OBS electronics appear in several records.

nized to the OBS clock, and one 40-s record is obtained per shot. This approach avoids possible contamination of the data by tape recorder vibration. In more recent experiments the record length has been increased to 80 s. Using amplifier gains and playback recorder sensitivities that give background signal amplitudes of 1–2 mm, magnifications of 3 million at 15 Hz are typically obtained in deepwater experiments.

The earthquake units are identical to the refraction units

TABLE 2. Layer Thicknesses h, Velocities v, and Intercept Times t_i

	Water		Sediment			Basement			Crust			Mantle		
Line	h, km	v, km/s	h, km	v, km/s	t_i, s	h, km	v, km/s	t_i, s	h, km	v, km/s	t_i, s	h, km	v, km/s	t_i, s
I	0.86	1.5	0.03	1.3	0.30		5.5	1.84						
			0.18	2.4	0.47									
			1.09	2.6	0.54									
			1.29	4.3	1.39									
II	2.63	1.5	0.12	2.2	1.28				4.9	6.0	2.71		8.1	3.82
			0.43	2.7	1.52									
			1.31	3.5	1.87									
IV	4.32	1.5	0.02	1.9	1.77		4.7	3.97						
			0.60	2.1	1.98									
			3.00	4.1	3.20									
V	4.84	1.5	0.30	2.0	2.08	0.48	5.4	4.37						
			1.35	2.4	2.72		5.6	4.40						
1N	2.31	1.5	0.73	2.5	1.23		5.9	3.13						
			2.27	3.4	1.77									
1S	2.32	1.5	0.33	2.1	1.10		5.9	3.13						
			3.00	3.6	1.65									
2	1.93	1.5	0.32	1.8	0.72		5.5	2.96						
			0.44	2.4	1.23									
			1.96	3.1	1.64									
3N	2.84	1.5	0.48	2.0	1.21	3.64	5.3	2.89					7.6	4.00
			1.22	3.2	2.05									
3S	2.8	1.5	1.48	2.0	1.26		5.0	3.1						
5	0.97	1.5	0.60	2.0	0.44		5.0	2.28						
			2.66	3.4	1.06									
6N	4.97	1.5	0.21	2.1	2.26									
			0.66	2.8	2.96									
				4.1	3.60									
6S	5.01	1.5	0.27	2.1	2.30									
			1.00	2.6	2.85									
				3.8	3.83									
7	4.31	1.5	0.20	2.0	1.90	2.35	5.3	3.37						
			1.08	3.6	2.78									
8N	2.80	1.5	0.60	2.9	1.59		5.2	2.62						
			1.60	4.1	2.04									
8S	2.84	1.5	1.39	3.2	1.67		5.3	2.52						
9						4.10	5.0	2.28	18.5	6.6	3.48		7.9	7.08
10	2.86	1.5				3.91	5.1	2.95	8.06	6.1	3.91		8.0	6.15
11	4.16	1.5	2.73	4.0	2.82				7.76	7.0	9.1		8.1	5.3

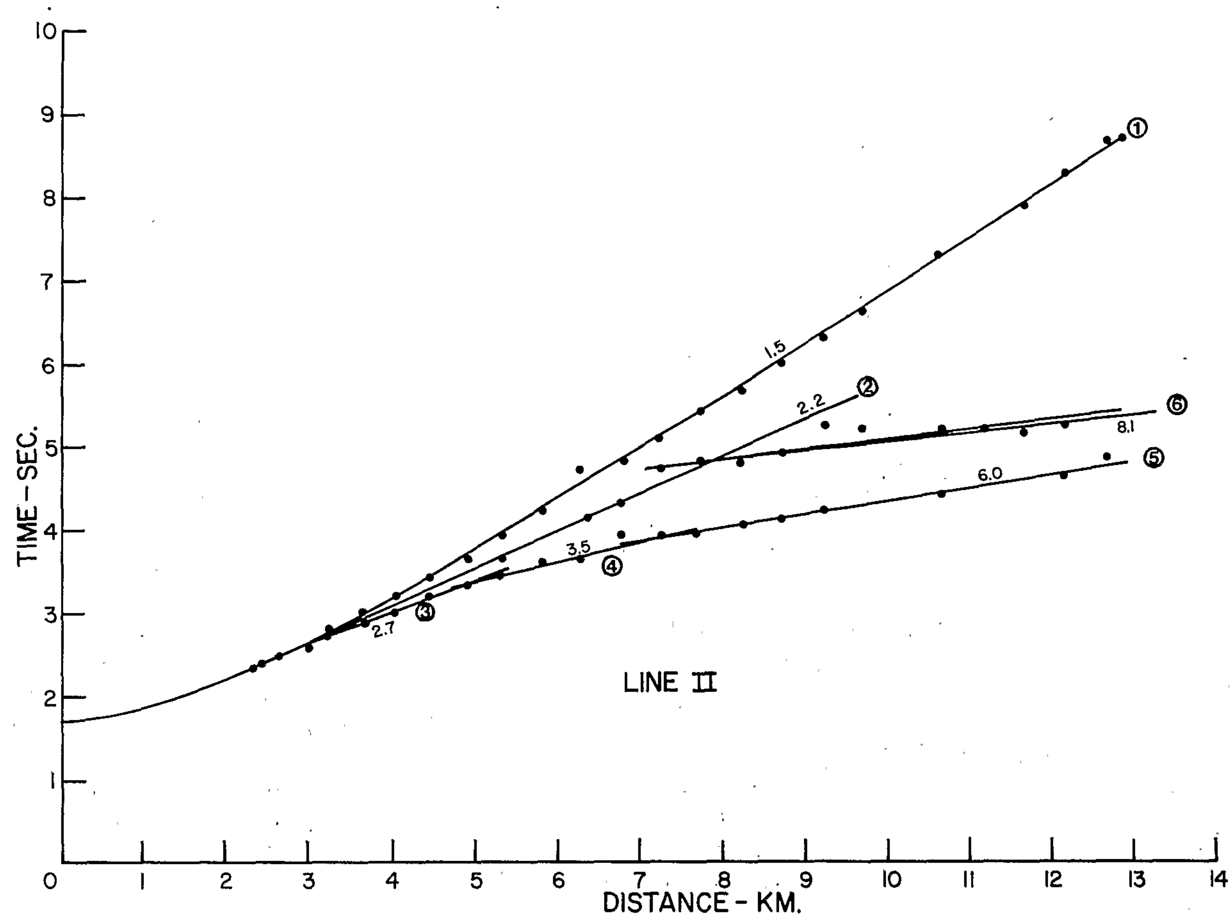

Fig. 7. Travel time curve for line II.

except that a 4.5-Hz geophone is substituted for the 8-Hz geophone, the record length is increased to 160 s, and the recorder is activated when the ratio of short-term signal power to long-term signal power exceeds a preset value.

DATA PROCESSING PROCEDURES

A distinct arrival corresponding to the direct water wave or its multiple can be identified in most of the records. Source-receiver distances were calculated from the water wave travel times. All data were corrected for water delay and topography.

Primary and secondary arrivals were identified in record sections of the type shown in Figure 2. Multiples of these arrivals in the water column were identified in some cases. All the data were bandpass-filtered through a 4- to 12-Hz window. Gain adjustment was applied to the data in 6-dB steps. The values of the gain used are shown on the record sections. A few of the signals in the record sections presented here, especially the water waves, are clipped owing to the higher gain used to enhance the ground arrivals. Travel times associated with linear segments of the corresponding travel time curves were fitted by the least squares, and layer thicknesses were calculated from the intercept times. The standard deviations in the least square fitting ranged between ±0.05 s and ±0.12 s, which could contribute to ±0.5 km in the layer thickness.

For lines I, II, IV, and V, adjustments in model parameters were made to provide the best fit between the theoretical and observed amplitude-distance curves. The theoretical amplitudes were calculated assuming geometrical ray theory approach [*Bullen*, 1959] and were compared with the amplitude of the first arrivals. The observed amplitude represents the measurements between the first peak and first trough of the signal. The calculations of the theoretical amplitude did not include absorption effects.

Examples of the record sections used for analysis are shown in Figure 2. We chose lines 7 and 8 because they demonstrate the marked difference in the characteristics of signals generated by an air gun (line 8) and that of an implosive (Flexichoc) source (line 7). The prolonged ring in the air gun sig-

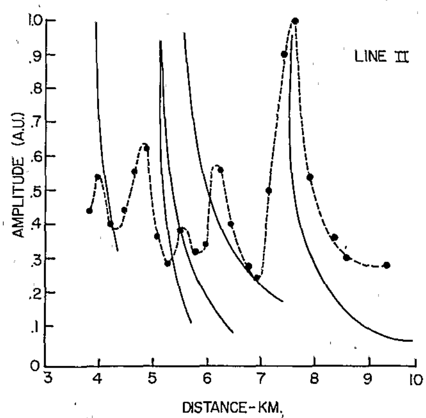

Fig. 8. Calculated (solid line) and observed first arrivals (dashed line) amplitude-distance curves for line II. The model used for calculation is shown in Figure 15.

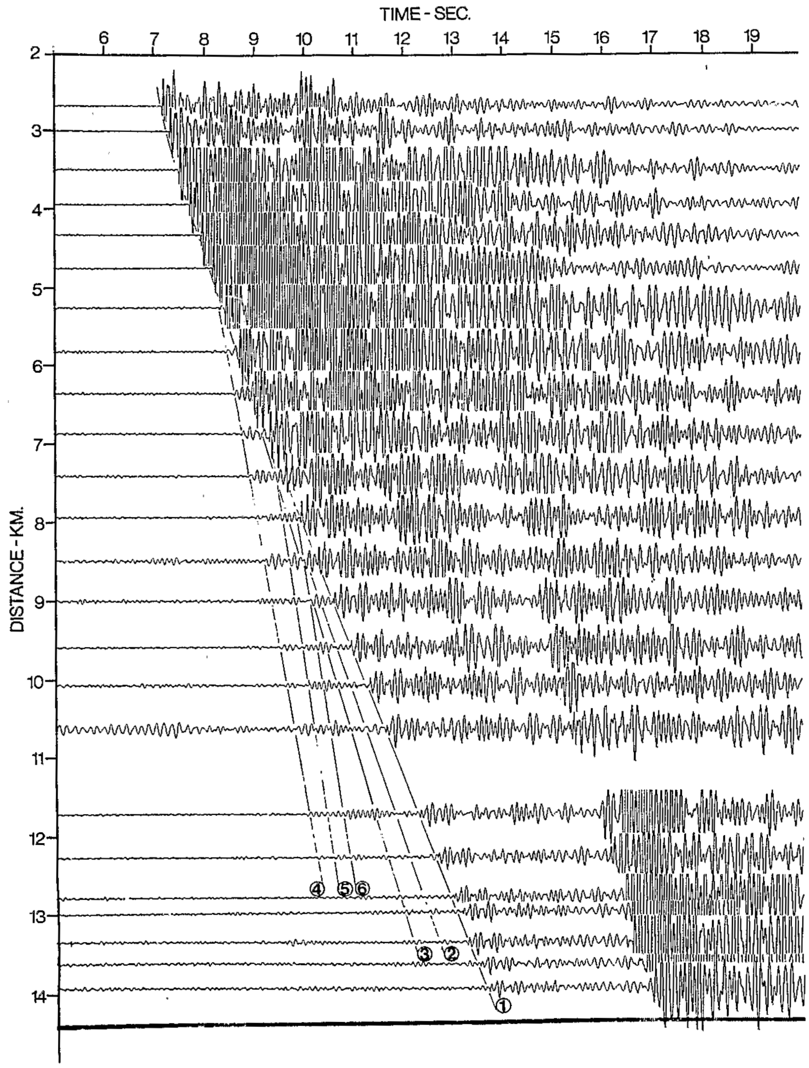

Fig. 9. Record section for line IV.

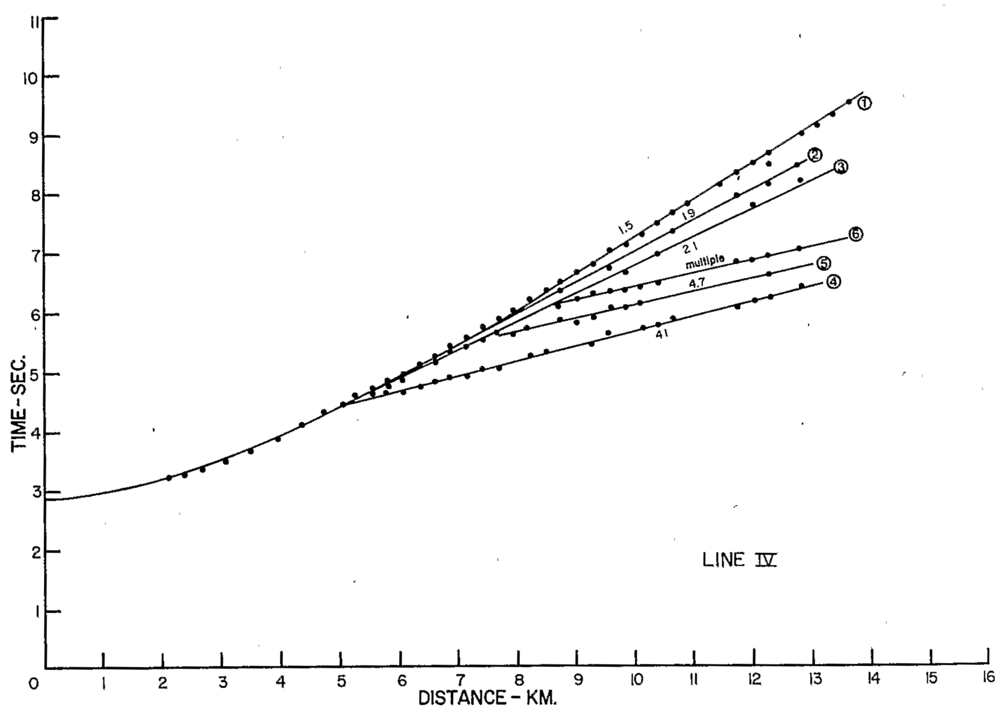

Fig. 10. Travel time curve for line IV.

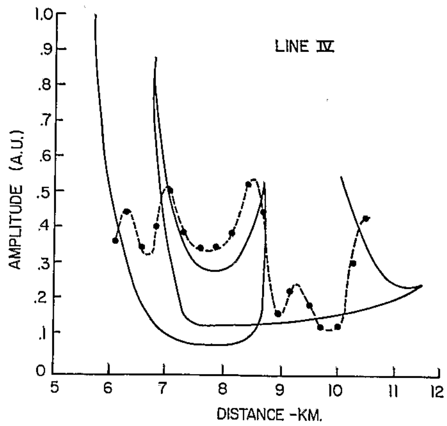

Fig. 11. Calculated (solid line) and observed first arrivals (dashed line) amplitude-distance curves for line IV. The model used for calculation is shown in Figure 15.

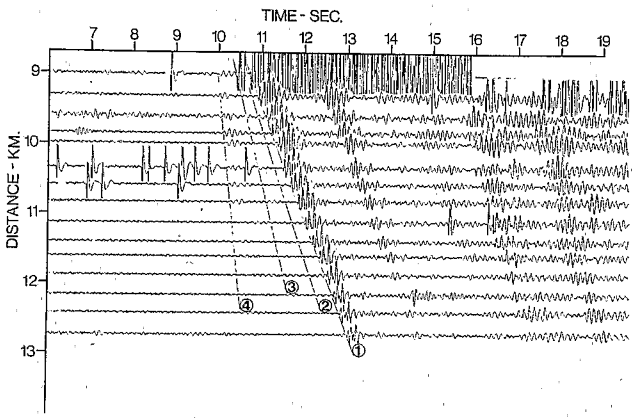

Fig. 12. Record section for line V. An OBS memory failure that began to develop at a distance of about 10.5 km prevented acquisition of short-range data in this profile.

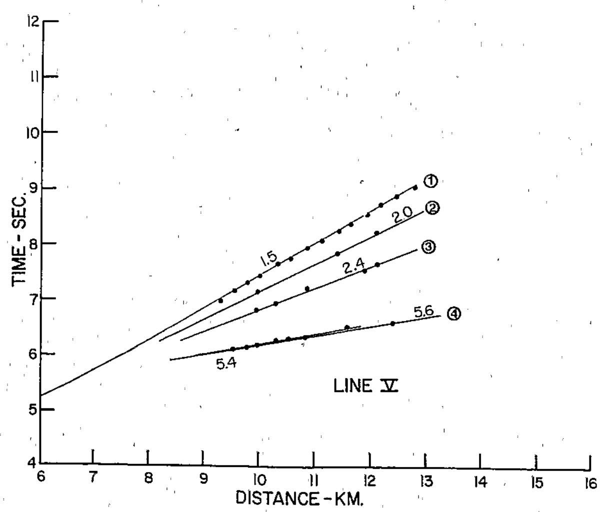

Fig. 13. Travel time curve for line V.

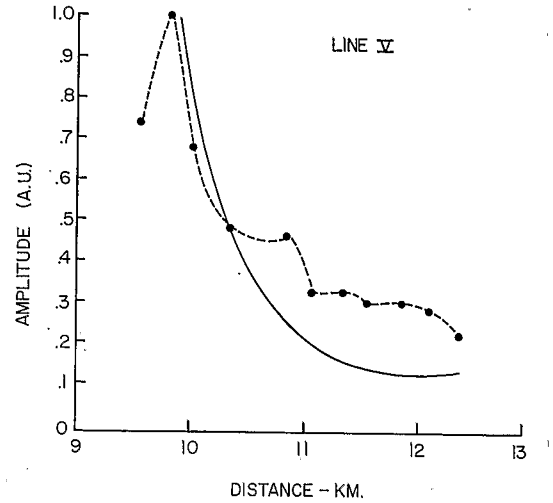

Fig. 14. Calculated (solid line) and observed first arrivals (dashed line) amplitude-distance curves for line V. The model used for calculation is shown in Figure 15.

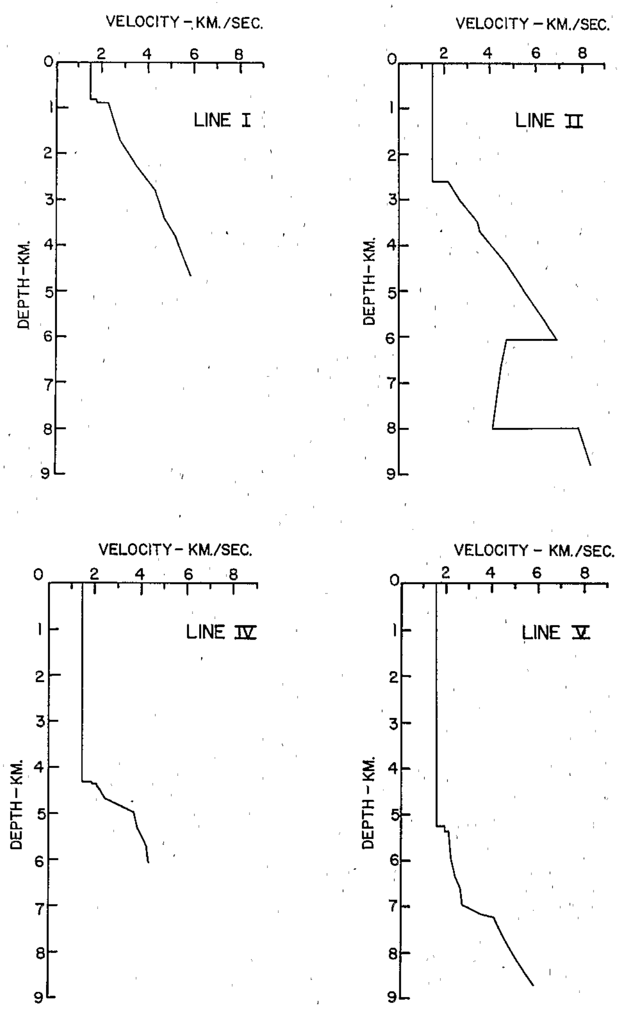

Fig. 15. Velocity-depth models derived from inversion of amplitude and travel time data. Models based upon travel time data only are given in Table 2. A low-velocity zone is required at the base of the crust to fit the travel time curve in line II.

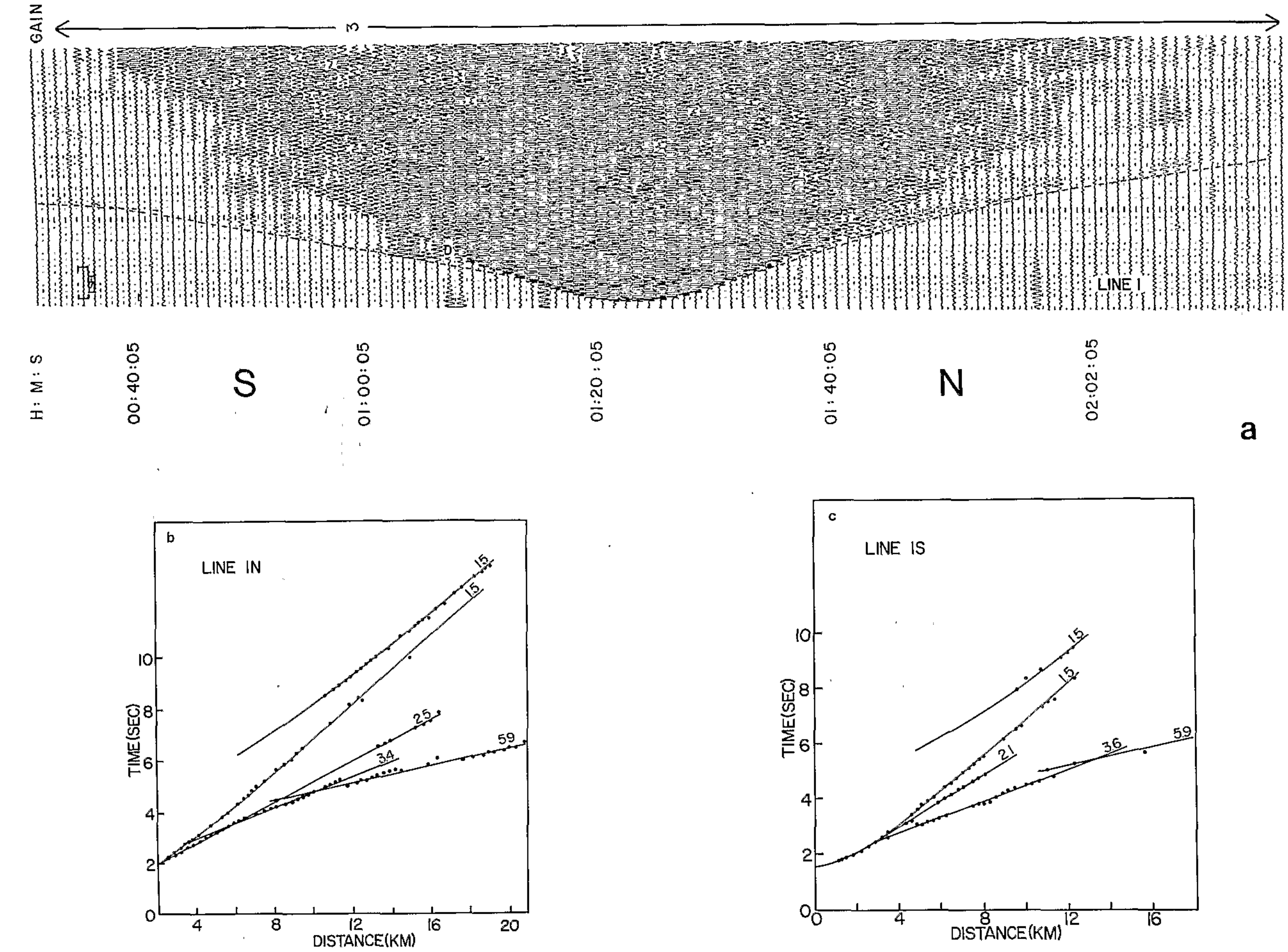

Fig. 16. (*a*) Record section for line 1. (*b*) Travel time curve for line 1, northern portion. (*c*) Travel time curve for line 1, southern portion. The variations in velocities between the northern and the southern portion of the section can be attributed to dipping layers.

nal, relative to the Flexichoc signal, is evident. We expect that the Flexichoc source would give superior data in high-resolution reflection work; however, the air gun was a more effective source in our refraction work because it generates greater energy at lower frequencies (about 10 Hz).

Data Description and Analysis

The OBS coordinates, energy source, time interval between shots, and maximum range of signal detection are listed for each line in Table 1. Lines III and 4 are omitted because the OBS malfunctioned in these two cases. Record sections, travel time curves, and theoretical and experimental amplitude-distance curves are given for lines I, II, IV, and V in Figures 3–14. The computed velocity models for these profiles are shown in Figure 15. The calculated amplitude-distance curves are based upon these models. These gradient models are approximated by layered models, and the composite section is shown in Figure 28. Record sections and travel time curves for lines 1–11 are shown in Figures 16–27. The record sections for these lines are plotted assuming the ship was steaming at a constant speed and the air gun was firing every minute. Assuming a ship speed of 8 knots (15 km/h), the separation between the traces in the record sections would be 0.25 km. The exact distances for plotting the travel time curves for these sections were calculated from the water wave. The velocities, intercept times, and calculated layer thicknesses for all lines are listed in Table 2. Explanatory remarks concerning individual lines, where needed, are included in the figure captions.

Discussion

The refraction results obtained in this study are combined in Figure 28 to produce a single profile along a line approximately perpendicular to the trench axis, and a close-up of the crustal structure is shown in Figure 29. Earthquakes hypocenters located from the data of the OBS and island station networks are included in the figure. The upper boundary of the inclined zone of seismic activity (Benioff zone) is indicated by a solid line. We also show inferred correlations of refracting horizons by solid lines. At depths greater than about 50 km the location of the Benioff zone is unambiguous. To define the extension of this zone toward the trench, we have assumed that peaks in the distribution of *S-P* time for earthquake signals recorded by the OBS stations correspond to the population of events originating along the nearest portions of the Benioff zone. Under this assumption, arcs drawn at distances given by *S-P* times corresponding to peaks in the *S-P* distri-

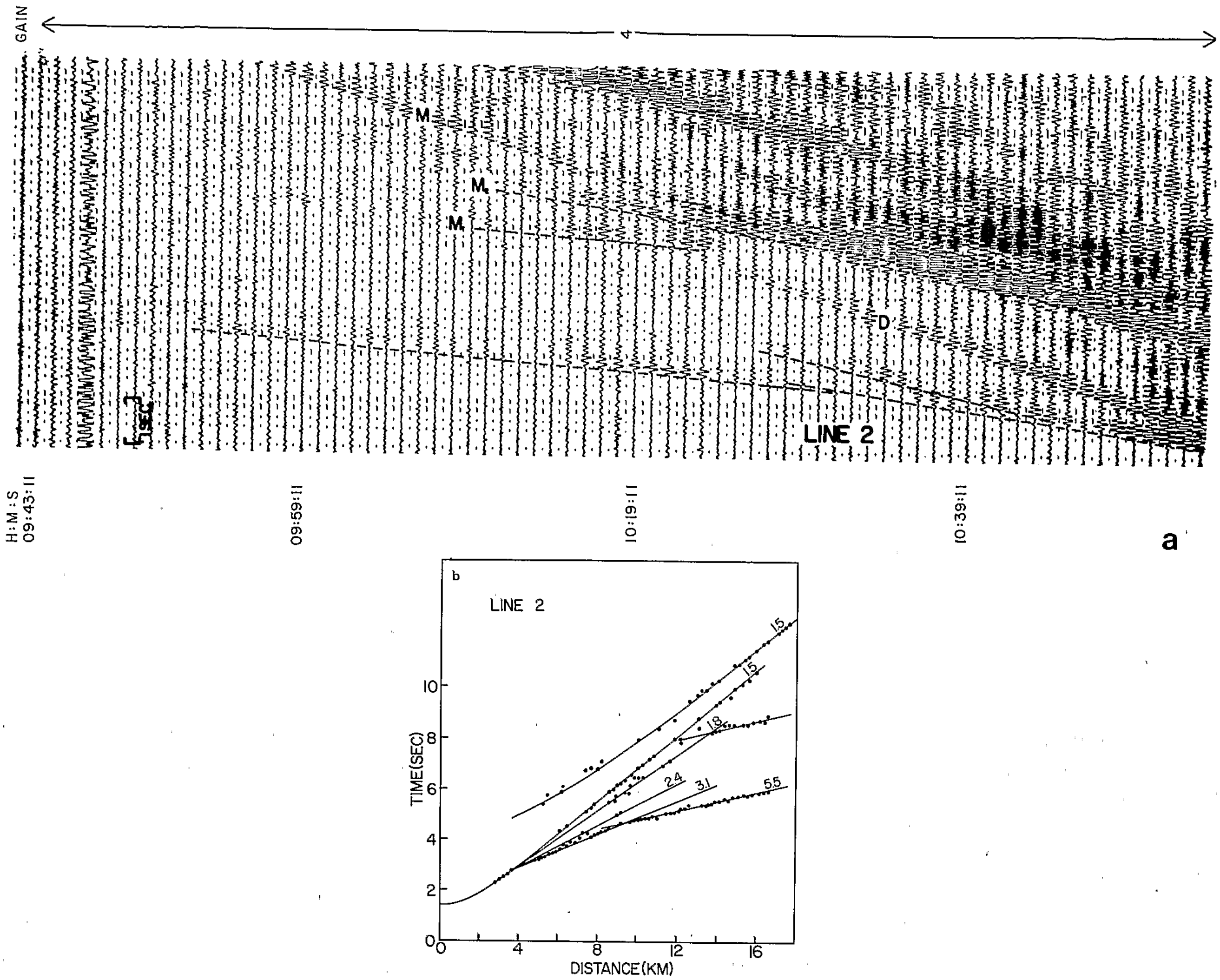

Fig. 17. (*a*) Record section for line 2. M_1 and M_2 represent multiple reflections of the 5.5-km/s and the 3.1-km/s ground arrivals in the water column, respectively. Small earthquake was recorded on trace 7. A constant gain factor of 4 was applied to the whole section. (*b*) Travel time curve for line 2.

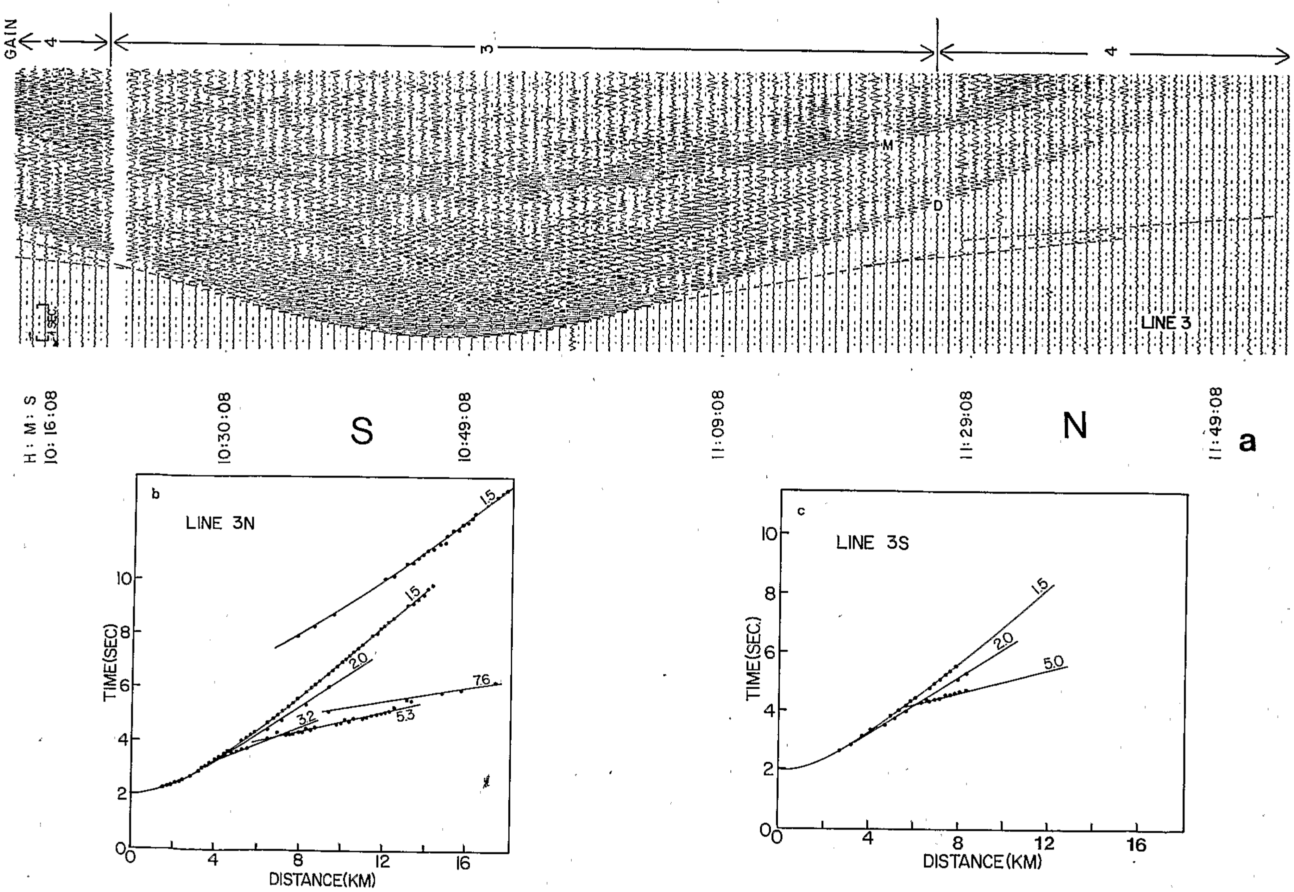

Fig. 18. (*a*) Record section for line 3. (*b*) Travel time curve for line 3, northern portion. (*c*) Travel time curve for line 3, southern portion.

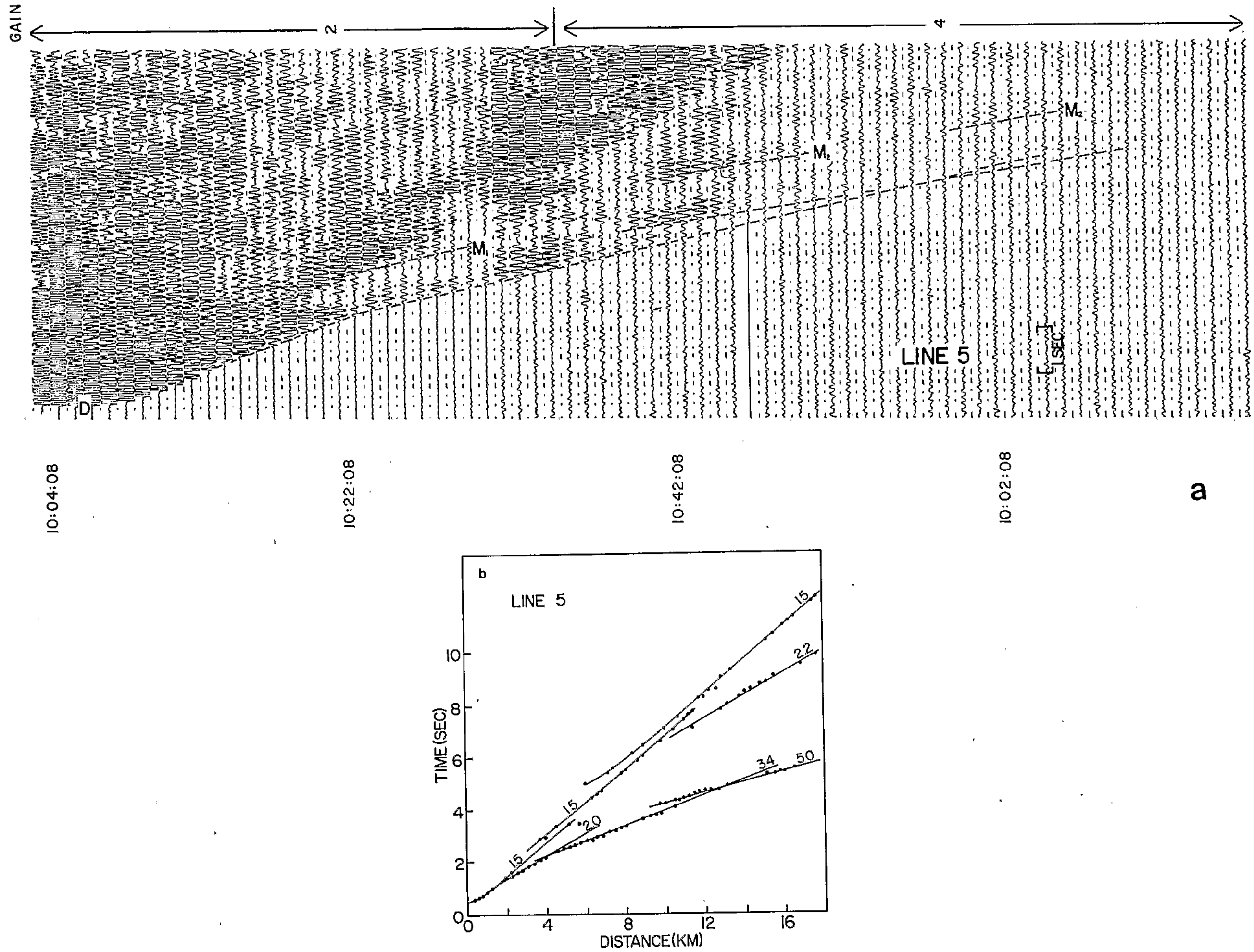

Fig. 19. (*a*) Record section for line 5. M_1 and M_2 represent multiple reflection of the 3.4-km/s and 5.0-km/s ground arrivals in the water column. The gain is increased by a factor of 12 dB after trace 28. (*b*) Travel time for line 5.

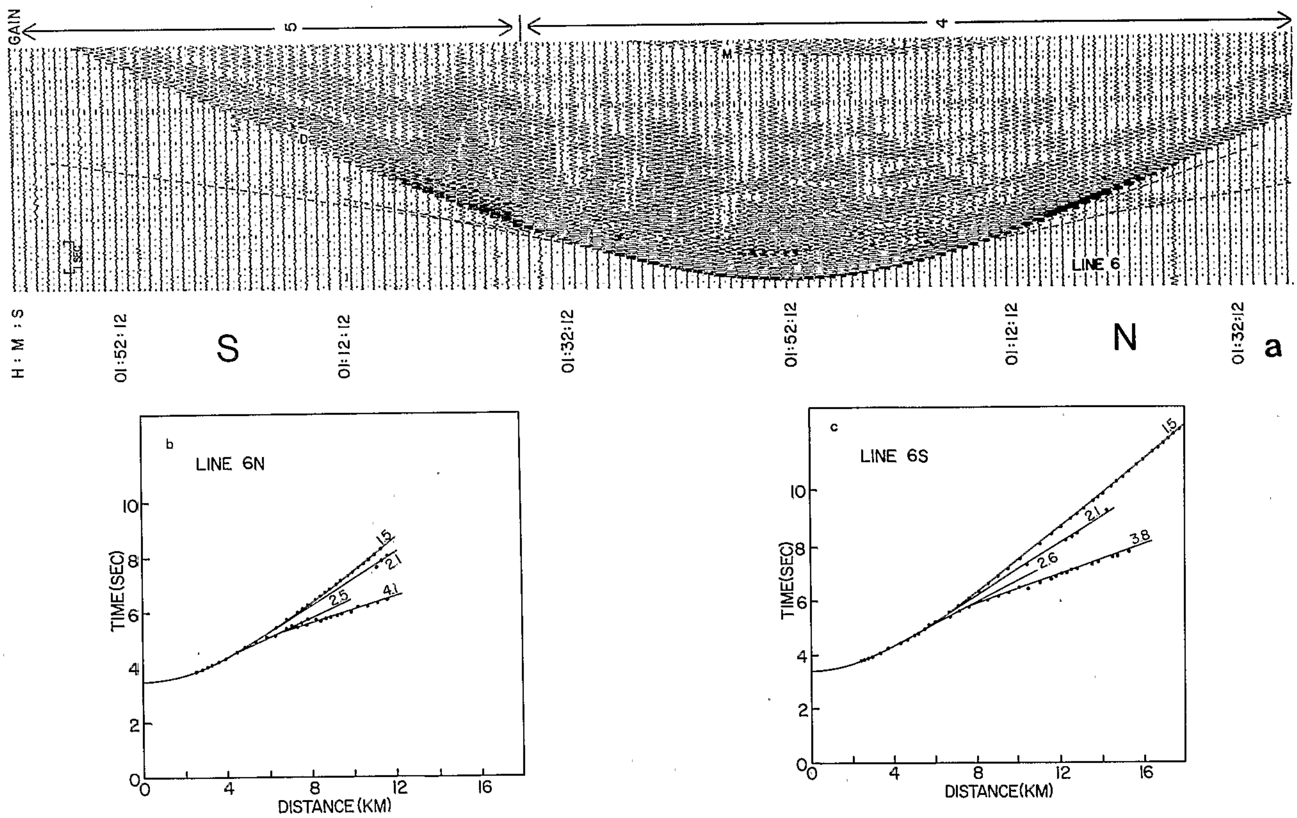

Fig. 20. (*a*) Record section for line 6. (*b*) Travel time curve for line 6, northern portion. (*c*) Travel time curve for line 6, southern portion.

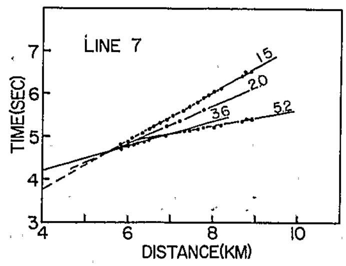

Fig. 21. Travel time curve for line 7.

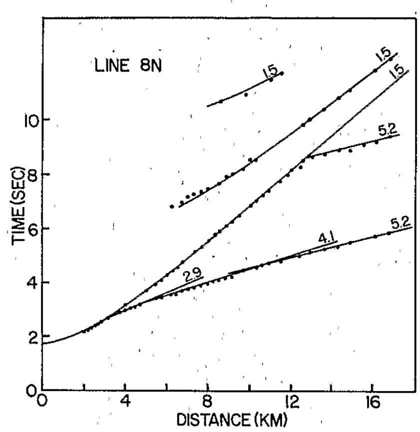

Fig. 22. Travel time curve for line 8, northern portion.

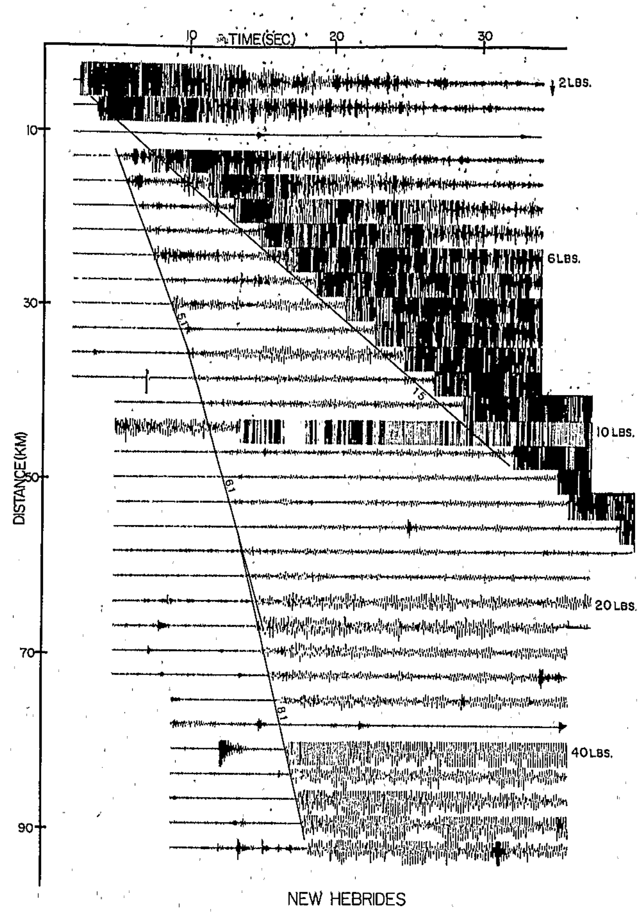

Fig. 24. Record section for line 10.

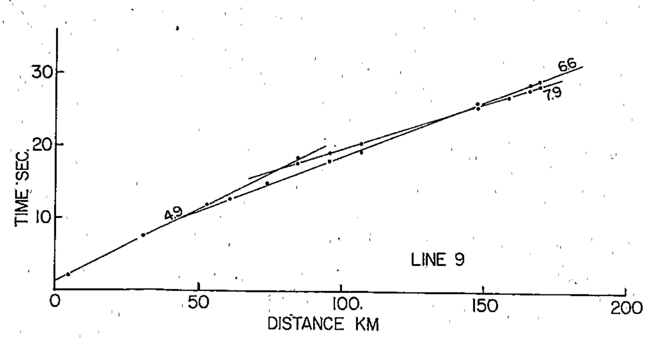

Fig. 23. Travel time curve for line 9. This line is recorded by a combination of OBS and island stations, as shown in Figure 1.

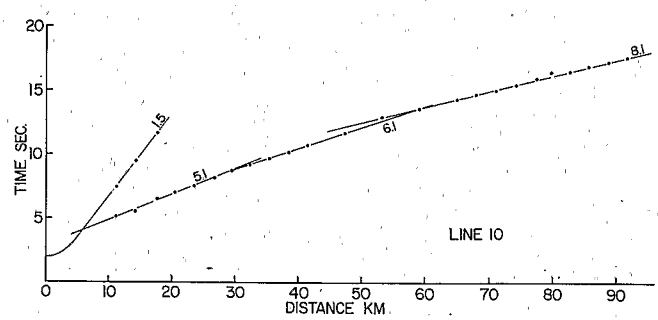

Fig. 25. Travel time curve for line 10.

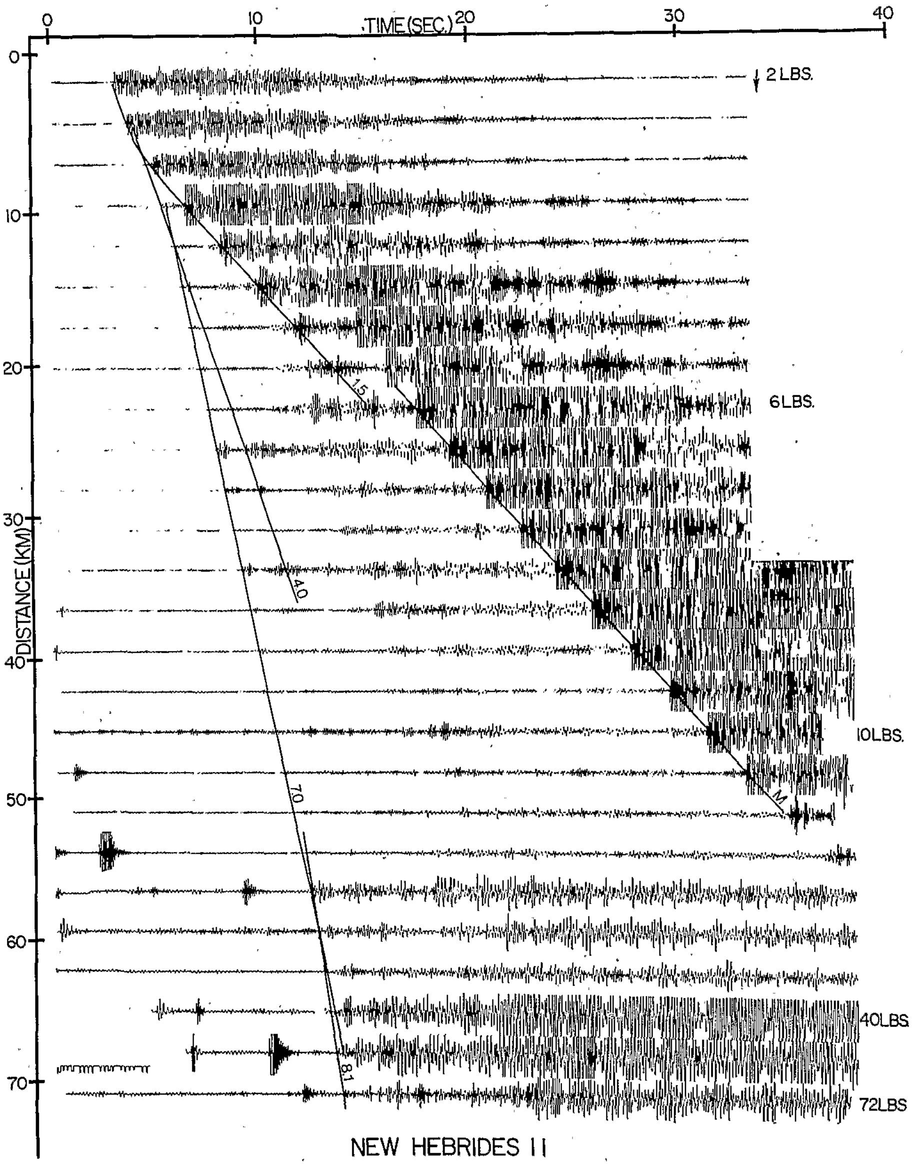

Fig. 26. Record section for line 11.

bution should pass through the Benioff zone. The arcs shown in Figure 28 appeared to define a reasonable extension of the Benioff zone to shallow depths. Arc 1 is derived from the data of OBS stations 5, 6, and 7. Arc 2 is derived from the data of OBS stations 3 and 4. The locations of OBS stations 2–7 are shown in Figure 1. Note that the profile velocities are used to calculate the arcs, so they are not segments of circles. The earthquake data supporting this result will be presented in a separate paper.

A maximum crustal thickness of 28 km is found beneath the New Hebrides island ridge. Models based upon gravity data place the depth to mantle beneath the islands at between 20 km [*Solomon and Biehler,* 1969] and 30 km [*Collot and Missègue,* 1976]. Although the oceanic crustal thickness at lines 7 and 11, located about 65 km west of the trench axis, is 10 km, which is substantially greater than that of typical oceanic crust [*Worzel,* 1974], the velocity of the basal layer (layer 3) is normal.

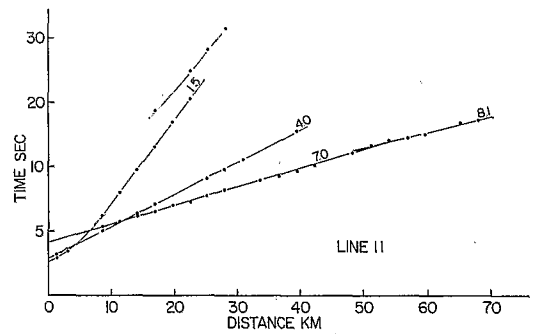

Fig. 27. Travel time curve for line 11.

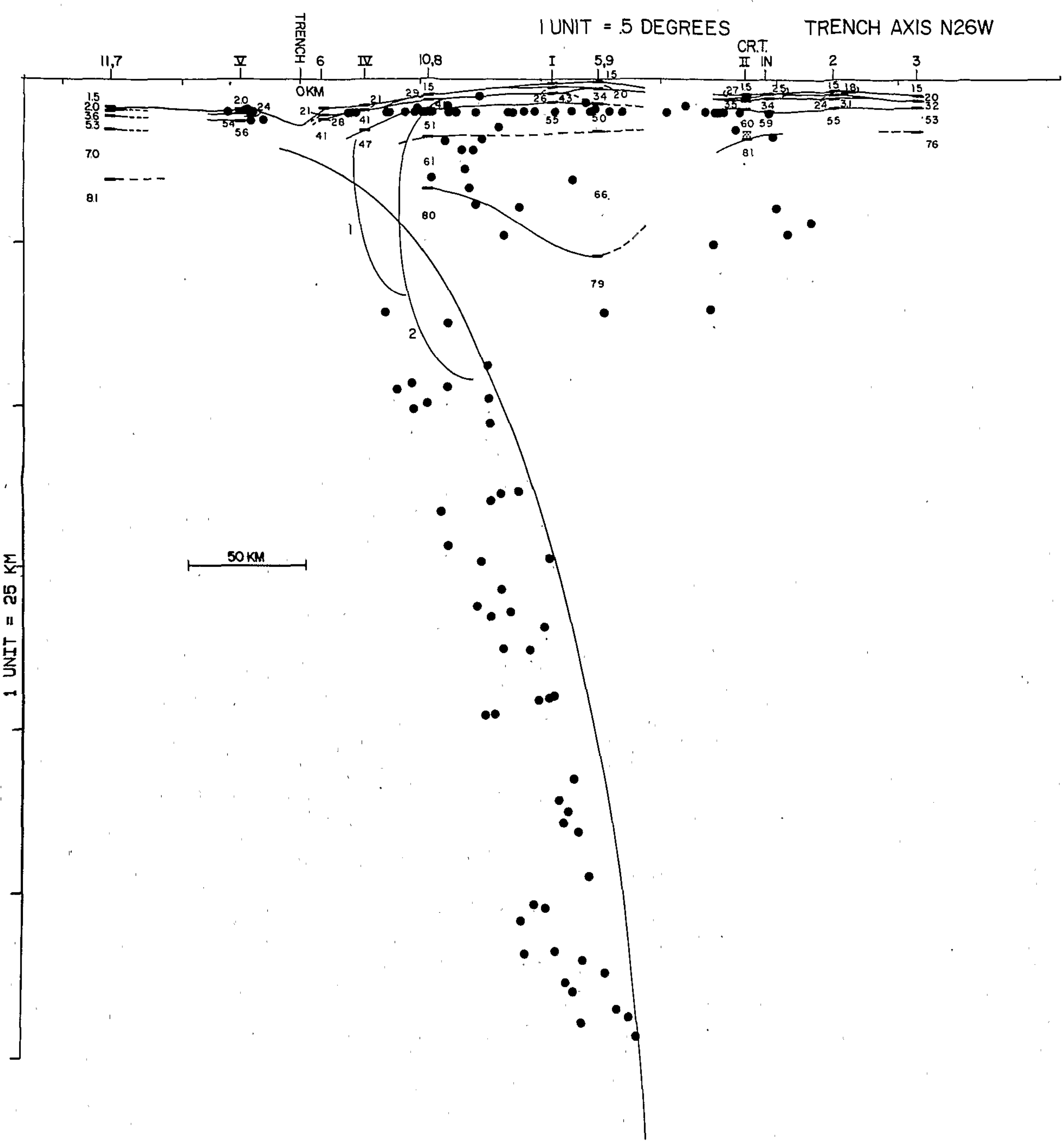

Fig. 28. Profile through central New Hebrides including all refraction results reported here. Well-located earthquakes are also included. Line numbers are indicated at the top of the figure. Locations of the earthquake OBS stations are also shown. Short arcs are the loci of points that define the Benioff zone based on peaks in S-P times of earthquake signals as described in the text. The stippled zone beneath line II indicates the low-velocity zone shown in Figure 15, and CRT refers to the Coriolis trough.

The crust thins to between 5 and 7 km beneath the Fiji Plateau (lines 2 and 3). On the basis of few data points the mantle velocity beneath line 3 is found to be 7.6 km/s. *Dubois et al.* [1973] also reported low mantle velocities (7.3–7.7 km/s) for earthquake phases crossing the southern Fiji plateau. *Shor et al.* [1971] obtained a velocity of 7.8 km/s in a refraction experiment at a location several hundred kilometers south of our study zone. On the basis of the relatively low upper mantle velocities, high seismic wave attenuation [*Barazangi et al.*, 1974], thin sediments, high heat flow [*McDonald et al.*, 1973], and low densities for the upper mantle from gravity data [*Solomon and Biehler*, 1969; *Dubois et al.*, 1973] suggest that the Fiji plateau is not an oceanic lithosphere belonging to the Pacific Ocean but is a recently generated plate.

The Coriolis trough (lines II and IN) is a seismically active back arc basin with local bathymetric relief of 1–2 km and a strong magnetic anomaly [*Dubois et al.*, 1978]. We find no evidence of substantial thinning or thickening of the crust beneath this feature; however, we note that the estimated depth to mantle beneath line II is based upon a relatively small

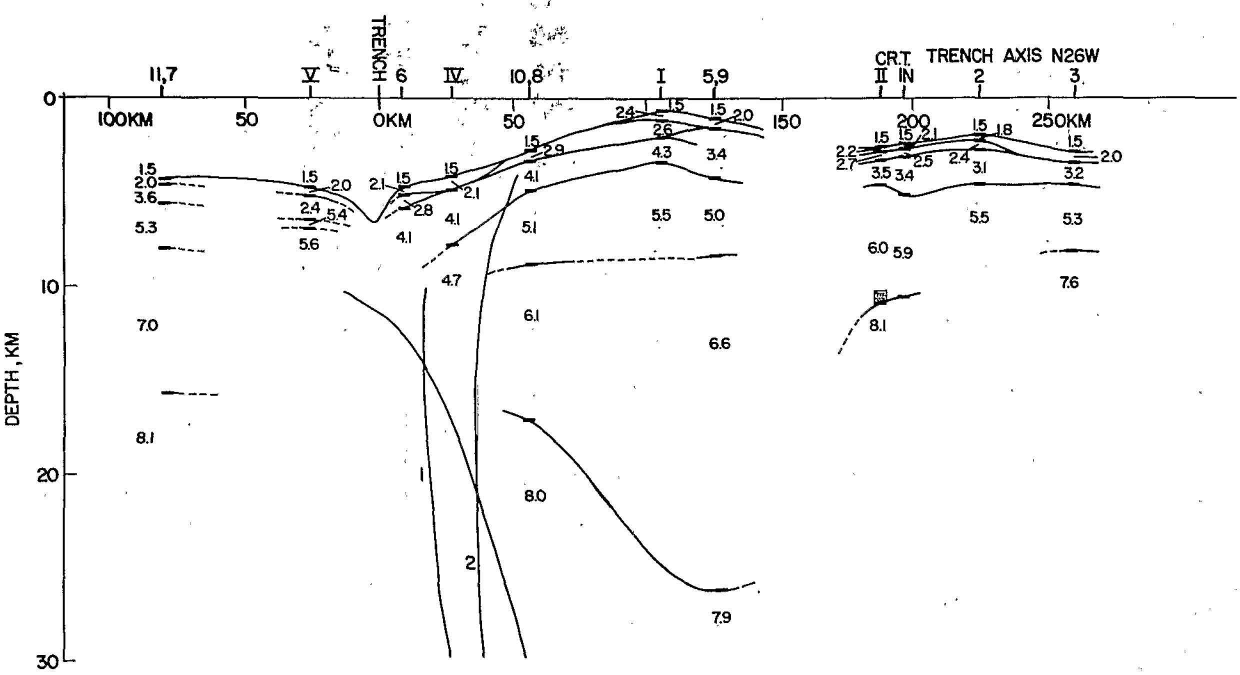

Fig. 29. Close-up of the crustal structure shown in Figure 28.

number of secondary arrivals, so the interpretation is open to question.

The present data are inadequate in the toe of the trench to determine the structure at depths greater than a few kilometers. In the shallow section, material with a velocity of 4.1 km/s forms a wedge that thickens toward the trench, beneath a thin surficial sediment layer. This material extends into, or very near to, the trench. This may be an accretionary deposit, or it may be of volcanic origin. We prefer to defer further speculation on this point until additional refraction data are available.

Acknowledgments. This work was supported by the Office de la Recherche Scientifique et Technique Outre-Mer, the National Science Foundation (grant EAR 75-14815), the U.S. Department of Interior (contract 14-08-0001-16703), the Henry L. and Grace Doherty Charitable Foundation, the National Oceanic and Atmospheric Administration (MO-A01-78-00-4120), and the Office of Naval Research (N00014-75-C-1121). We are grateful to Jacque Dubois for assistance in planning the experimental strategy, to James Dorman and John Ladd for reviewing the manuscript and offering helpful suggestions, and to Yosio Nakamura for providing the software for digitizing and plotting the analogue tapes. We would also like to acknowledge CNEXO (Technique Outre-Mer, the Centre National pour l'Exploitation des Océans, The National Science) for providing the Flexichoc source and the ship time for the experiment.

REFERENCES

Barazangi, M., B. Isacks, J. Dubois, and G. Pascal, Seismic wave attenuation in the upper mantle beneath the southwest Pacific, *Tectonophysics, 24,* 1–12, 1974.

Bullen, K. E., *Introduction to the Theory of Seismology,* 296 pp., Cambridge University Press, New York, 1959.

Collot, J., and F. Missegue, Crustal structure between New Caledonia and the New Hebrides, paper presented at the International Symposium of Geodynamics in Southwest Pacific, Office de la Rech. Sci. et Tech. Outre-Mer, Noumea, New Caledonia, Aug. 27–Sept. 2, 1976.

Dubois, J., G. Pascal, M. Barazangi, B. Isacks, and J. Oliver, Travel times of seismic waves between the New Hebrides and Fiji Islands: A zone of low velocity beneath the Fiji Plateau, *J. Geophys. Res., 78,* 3431, 1973.

Dubois, J., F. Dugas, A. Lapouille, and R. Louat, The trough at the rear of the New Hebrides island arc: Possible mechanism of formation, *Can. J. Earth Sci., 15,* 351–360, 1978.

Ibrahim, A. K., and G. V. Latham, A comparison between sonobuoy and ocean bottom seismograph data and crustal structure of the Texas shelf zone, *Geophysics, 43,* 514, 1978.

Latham, G., P. Donoho, K. Griffiths, A. Roberts, and A. K. Ibrahim, The Texas ocean bottom seismograph, paper presented at the Offshore Technology Conference, Soc. of Explor. Geophys., Houston, Tex., 1978.

MacDonald, K. C., B. P. Luyendyk, and R. P. Von Herzen, Heat flow and plate boundaries in Melanasia, *J. Geophys., 78,* 2537, 1973.

Shor, G. G., H. K. Kirk, and H. W. Menard, Crustal structure of the Melanesian area, *J. Geophys. Res., 76,* 2562, 1971.

Solomon, S., and S. Biehler, Crustal structure from gravity anomalies in the southwest Pacific, *J. Geophys. Res., 74,* 6696, 1969.

Worzel, J., Standard oceanic and continental structure, in *The Geology of Continental Margins,* edited by C. A. Burk and C. L. Drake, pp. 59–66, Springer, New York, 1974.

(Received April 12, 1979;
revised July 23, 1979;
accepted August 13, 1979.)